

Article

Real-Time Process Monitoring Based on Multivariate Control Chart for Anomalies Driven by Frequency Signal via Sound and Electrocardiography Cases

Chih-Hung Jen ¹  and Chien-Chih Wang ^{2,*} 

¹ Department of Information Management, Lunghwa University of Science and Technology, Taoyuan City 333326, Taiwan; f7815@mail.lhu.edu.tw

² Department of Industrial Engineering and Management, Ming Chi University of Technology, New Taipei City 243303, Taiwan

* Correspondence: iecchwang@mail.mcut.edu.tw; Tel.: +886-2-2908-9889

Abstract: Recent developments in network technologies have led to the application of cloud computing and big data analysis to industrial automation. However, the automation of process monitoring still has numerous issues that need to be addressed. Traditionally, offline statistical processes are generally used for process monitoring; thus, problems are often detected too late. This study focused on the construction of an automated process monitoring system based on sound and vibration frequency signals. First, empirical mode decomposition was combined with intrinsic mode functions to construct different sound frequency combinations and differentiate sound frequencies according to anomalies. Then, linear discriminant analysis (LDA) was adopted to classify abnormal and normal sound frequency signals, and a control line was constructed to monitor the sound frequency. In a case study, the proposed method was applied to detect abnormal sounds at high and low frequencies, and a detection accuracy of over 90% was realized. In another case study, the proposed method was applied to analyze electrocardiography signals and was similarly able to identify abnormal situations. Thus, the proposed method can be applied to real-time process monitoring and the detection of abnormalities with high accuracy in various situations.

Keywords: statistical process control; empirical mode decomposition; intrinsic mode functions; linear discriminant analysis



Citation: Jen, C.-H.; Wang, C.-C. Real-Time Process Monitoring Based on Multivariate Control Chart for Anomalies Driven by Frequency Signal via Sound and Electrocardiography Cases. *Processes* **2021**, *9*, 1510. <https://doi.org/10.3390/pr9091510>

Academic Editor: Jae-Yoon Jung

Received: 1 July 2021

Accepted: 24 August 2021

Published: 26 August 2021

Publisher's Note: MDPI stays neutral with regard to jurisdictional claims in published maps and institutional affiliations.



Copyright: © 2021 by the authors. Licensee MDPI, Basel, Switzerland. This article is an open access article distributed under the terms and conditions of the Creative Commons Attribution (CC BY) license (<https://creativecommons.org/licenses/by/4.0/>).

1. Introduction

Network technology, cloud computing, and big data analysis are being gradually integrated with industrial automation in a digital transformation known as Industry 4.0. For example, the Internet of Things can be used to develop a smart monitoring system to enhance the transparency and automate the operation of a factory. Process monitoring involves analyzing non-structuralized data and combining them with structuralized data to determine potentially important parameters. However, many problems regarding procedure combination and information classification still need to be resolved.

In the field of process monitoring, fault detection and diagnosis (FDD) is focused on detecting abnormal situations, done through modeling, signal processing, and intelligence computation. The FDD methods can generally be classified into three categories: model-based online data-driven methods, signal-based methods, and knowledge-based history data-driven methods [1]. Yan et al. proposed a hybrid method to detect faults for chiller subsystems, only using the normal data to implement the training procedure. This online monitoring framework was constructed to use an extended Kalman filter (EKF) model with a recursive one-class support vector machine (ROSVM) [2]. Sun et al. presented a hybrid RCA fault diagnosis model combined support vector machine (SVM) with wavelet de-noising (WD) and an improved max-relevance and min-redundancy (mRMR)

algorithm for dealing with the complexity of variable refrigerant flow (VRF) systems [3]. Rogers et al. reviewed and evaluated state-of-the-art methods for performing FDD for air conditioning systems. Herein, the emerging field of fault detection for residential air conditioning systems was also reviewed by using cloud-based thermostat data [4]. Gangsar and Tiwari reviewed the conventional time and spectrum signal analyses for the two most effective types of signals (the vibration and various induction motor (IM) faults). The existing research and development in the field of signal-based automation of condition monitoring methodologies for the FDD of various electrical and mechanical faults were also summarized and evaluated [5]. Neupane and Seok summarized the recent works for evaluating the applications in deep learning algorithms; this study also used the Case Western Reserve University (CWRU)-bearing dataset in machinery fault detection and diagnosis [6].

In semiconductor processes, Fan et al. proposed an anomaly detection method that used a denoise autoencoder (DAE) to learn the primary representation of normal wafers from equipment sensor readings and serve as the one-class classification model. Next, the Hampel identifier, a robust method of outlier detection, was also adopted to determine a new threshold for detecting defective wafers, called MaxRE without outlier (MaxRE-wo) [7]. Data visualization is applied to transform original data, highlight the process trends and outliers by using the data in an easy-to-understand format, and help researchers comprehend the data's relevance. Visualization tools enable practitioners to transform every element of the data into interactive charts and pictures. Fan et al. utilized the texture analysis technique with 2-D Fourier transform to analyze images of the critical parameters for detecting defective wafers [8].

In the precision machining industry, the automatically productive equipment frequently needs to execute tool processing, such as turning, cutting, drilling, grinding, and so forth. However, most abnormal situations in these processes are from the extensive tool wear, and the motors (or transmission mechanisms) in the equipment generate the abnormalities; these abnormal situations often accompany the abnormal sound frequency. Speech frequencies and other electronic signals have been studied for more than three decades to understand sound signals' anomalous nature. Xu and Jon applied traditional multivariate analysis to sound frequency estimation and proposed combining sound frequency and video signals to estimate the acoustic signal-to-noise ratio (SNR) [9]. Xie and Cao improved the Mel-frequency cepstral coefficients (MFCCs) to significantly reduce the computation and strengthen the hardware execution of sound frequency monitoring [10]. Nalini et al. applied sound frequency identification to a biometric recognition system to address loopholes in existing vision-based and sensor systems. They achieved a failure rate of 19.09%, which was slightly less than that of the existing NARX/HM system (20.91%) [11]. Nalini applied MFCCs and a residual phase to develop a model for identifying emotions in music. Furthermore, they used an absolute artificial neural network (AANN), a support vector machine (SVM), and a radial basis function (RBF) network to classify the music archives of different websites and achieved identification rates of 96.0%, 99.0%, and 95.0%, respectively [12]. Lee et al. proposed an audio-based event detection system to monitor the safety of workers and rapidly identify construction accidents [13]. Liu and Li presented a construction sound monitoring system with a double-layer identification scheme consisting of two random forest-based classifiers to prevent damage to underground pipelines. They were able to detect 95.59% of all threat signals [14]. For healthcare, Wei et al. applied adaptive support vector regression and weighted-index average algorithms to calculate fetal heart rates [15].

If the abnormal sound frequency with the critical process parameters can be utilized, it will define the process fault quickly, and the engineer can execute the proper operation. In addition, the production machine can maintain a stable vibration in advanced semiconductor processes, which is also critical for process quality. Many device anomalies can be identified by sound and vibration frequencies; thus, the efficiency of such monitoring systems can be further improved if portable radios are combined with algorithms for quick

anomaly detection. Based on two such monitoring requirements, we used two cases of similarity signals (sound frequency and electrocardiography) to implement the monitoring of frequency signals and to evaluate its feasibility in practical application. Moreover, the monitoring in advanced processes needs a quick response and to display a simple visualization. Thus, the complicated frequency signals are converted to form a curve via the multiscale entropy (MSE) method, and the concept of profile monitoring is used to implement the monitoring task. Using the fitting model of the MSE curve, the model parameters for different curves can be obtained and linear discriminant analysis (LDA) is applied to execute the classification of an abnormal situation. When the parameters of abnormal classification are decided, the Hotelling T^2 control chart can be established to implement the monitoring of frequency signals. The advantage of such an operation is to convert the complicated frequency signals and form a more accessible control chart. Thus, the process engineer can quickly evaluate the abnormal situation and adopt the appropriate treatment to achieve online monitoring.

2. Methodology

The focus of this study was the construction of a real-time monitoring system that can quickly identify abnormalities based on a sound frequency signal. The empirical mode decomposition (EMD) method was first applied to decompose the original sound frequency signal and generate the different frequency domains of intrinsic mode functions (IMFs). Using the screening feature IMFs, the frequency signal is reconstructed to remove the noise and increase the detective effect. Next, the sample entropies (SampEn) for different scales are calculated using the recombined feature signal, and some sample points are produced to fit the appropriate model for the MSE curve. In terms of these model parameters, Hotelling's T^2 control chart is constructed, and then LDA is applied to determine the control limit to monitor the abnormal sound frequency signal.

2.1. Decomposition of Sound Frequency Signals

EMD is applicable to nonlinear and unstable data, such as sound frequency signals. EMD utilizes characteristic time scales in signals to define the vibrational modes [8]. A non-zero mean signal can also be used, and the decomposition procedure is called the sifting process. The sifting process is applied to obtain the IMFs of the original signal. Some IMFs have physical features that can be used for further analysis. The obtained IMFs are checked to determine whether they meet the given constraints. If they do, the sifting process continues to obtain the next group of IMFs. This process is repeated until all IMFs that meet the constraints are obtained [16–19]. The last group of IMFs exhibits the trend of the mean. Hence, the sifting process aims to eliminate the carrier waves of signals to achieve a more symmetric waveform, as follows [20,21]:

1. Determine the partial maxima and minima of the original signal $X(t)$. Then, use a cubic spline to connect the maxima to form an envelope and connect the minima to form another envelope. Aggregate and average the two envelopes to obtain the mean envelope $m_1(t)$. Subtract $m_1(t)$ from $X(t)$ to obtain the vector $h_1(t)$:

$$X(t) - m_1(t) = h_1(t) \quad (1)$$

2. Check if $h_1(t)$ meets the constraints for the IMFs. If it does, return to Step (1), and take $h_1(t)$ as the original signal for the second sifting process to obtain $h_{11}(t)$:

$$h_1(t) - m_{11}(t) = h_{11}(t) \quad (2)$$

3. After the sifting process is repeated k times, the original signal $X(t)$ meets the constraints and becomes the IMF vector $h_{1,k}(t)$:

$$h_{1,k-1}(t) - m_{1,k}(t) = h_{1,k}(t) \quad (3)$$

4. Excessive sifting eliminates the original physical meaning. Hence, the following conditions are set for convergence to ensure that the IMFs maintain the original vibration amplitude and physical meaning:

- The number of zero-crossing points must be equal to that of the partial extrema (i.e., the partial maxima and partial minima), and the standard deviation (SD) should be between 0.2 and 0.3:

$$SD = \sum_{i=0}^T \left[\frac{(h_{1,k-1}(t) - h_{1,k}(t))}{h_{1,k-1}} \right]^2 \quad (4)$$

- If one of the conditions is met, the sifting process is complete, and the first IMF vector $c_1(t)$ is obtained. $c_1(t)$ is the shortest cycle of the entire set of signals:

$$c_1(t) = h_{1,k}(t) \quad (5)$$

5. Subtract $c_1(t)$ from $X(t)$ to obtain the complementary function $r_1(t)$:

$$X(t) - c_1(t) = r_1(t) \quad (6)$$

6. If $r_1(t)$ contains a longer cycle vector, repeat steps 1–5 to continue sifting and decompose it into n (cardinal number) IMF vectors $c_n(t)$:

$$\begin{aligned} r_1(t) - c_2(t) &= r_2(t) \\ &\vdots \\ r_{n-1}(t) - c_n(t) &= r_n(t) \end{aligned} \quad (7)$$

7. If $r_n(t)$ cannot be decomposed into IMF vectors, the sifting process is suspended. The final $r_n(t)$ is the mean trend. All IMF vectors $c_n(t)$ are aggregated with the mean trend to obtain the original signal $X(t)$. Combine Equations (6) and (7) to obtain

$$X(t) = \sum_{k=1}^n c_k(t) + r_n(t) \quad (8)$$

After the above decomposition of the IMF vectors, the IMFs are classified and combined with correlating different sound frequencies with process abnormalities. Herein, the significant IMF vectors for distinguishing the abnormalities can be selected and reconstructed to form a recombined feature signal.

2.2. Recombination and Monitoring of Signals

The obtained IMFs can be used to select highly identifiable functions for recombination and recognize abnormal sound frequencies. The profile monitoring theory was adopted using the recombined feature signal to analyze sound frequencies for abnormalities. MSE was used to convert the recombined feature signal. It adopts the concept of multiple scales to calculate and represent complexity properly rather than causing any deviation. In addition, it can be used to observe trends of complexity on different scales. The basic principles of MSE are based on approximate entropy and sample entropy (SampEn). The recombined feature signal from the sound frequency data are preprocessed, where the time sequence data entries are shortened. Then, the approximate entropy or sample entropy is added to calculate the entropy. The basic structure of MSE is presented in Figure 1 [22].

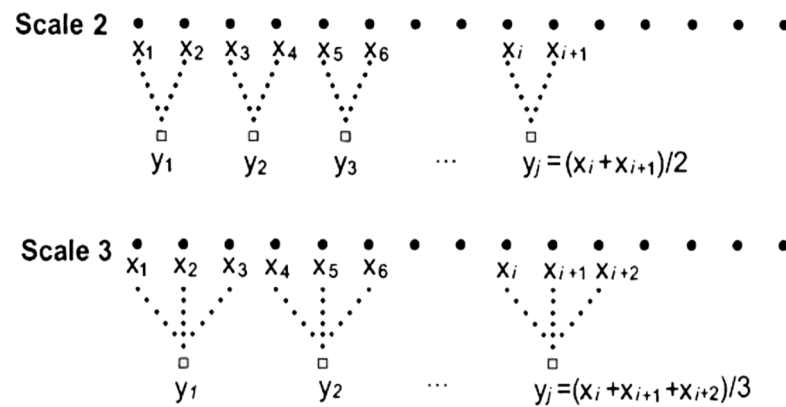


Figure 1. Coarse-graining procedure of multi-scale entropy.

The recombined feature signal for the coarse-graining procedure is presented in Figure 1. The values of every two points are averaged to obtain another group of the sequence. Then, the sample entropy for Scale 2 is calculated, as presented in Equation (9). Then, the values of every three points are averaged to obtain another group of the sequence, and the sample entropy for Scale 3 is obtained in the same manner. Thus, the sample entropies (SampEn) can be obtained for different time scales, which are aggregated to obtain the complexity index (CI):

$$\text{SampEn}(m, r, N) = -\ln \frac{\sum \frac{C_{i,m+1}}{N-m-1}}{\frac{C_{i,m}}{N-m}} \quad (9)$$

$$\text{CI} = \sum_{i=1}^N \text{SampEn}(i), \quad i = \text{scale factor}, \quad n = \text{total scale} \quad (10)$$

In this study, each feature signal was computed to generate 20 sample points from Scales 1–20 using Equation (9). The 20 sample points were then fitted to use the polynomial regression model (or the sum of sine functions) and obtain the model parameters of the MSE curve. Then, MSE converted the feature frequency signals into the profile graph presented in Figure 2. The profiles were then used to classify abnormalities in the sound frequency signals to construct the monitoring framework.

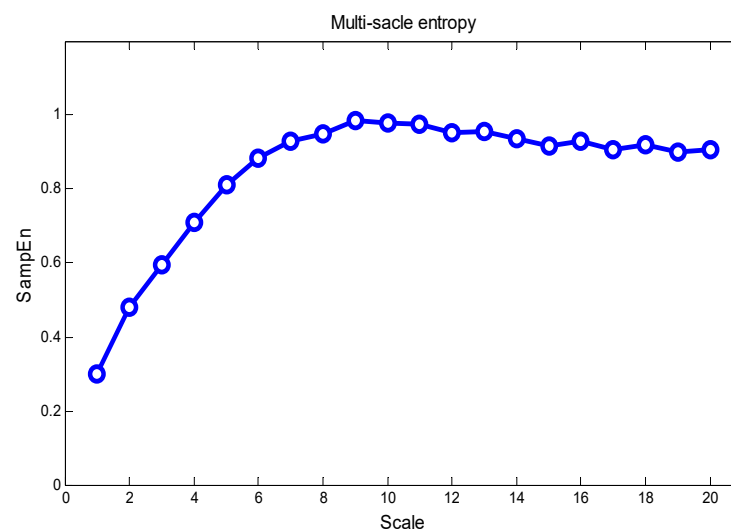


Figure 2. Converted MSE curve.

2.3. Apply Hotelling T^2 and Linear Discriminant Analysis to Sound Frequency Monitoring

When the MSE curve was formed and to obtain the model parameters ($\hat{\beta}$), Hotelling's T^2 control chart was established, and the LDA was then used to determine the control limit to monitor and to distinguish the abnormal signals. The obtained profiles were used to simulate monitoring of the sound frequency signal for abnormalities at different scales. First, the sample points of the MSE curve were fitted into an appropriate model. Herein, the polynomial regression model and the sum of sine functions were used to construct the profile model. The polynomial model with a single explanatory variable is described as

$$y_j = \beta_0 + \sum_{r=1}^k \beta_r x_j^r + \varepsilon_j, \quad r = 1, \dots, k; j = 1, \dots, n \quad (11)$$

where β_0 and β_r are the unknown parameters of the polynomial function and r is the order of the polynomial. The modified sum of sine functions is represented as

$$y_j = \sum_{r=1}^k \mathbf{a}_r \sin(\mathbf{b}_r \mathbf{x}_j + \mathbf{c}_r) + \varepsilon_j, \quad r = 1, \dots, k; j = 1, \dots, n \quad (12)$$

In Equation (12), \mathbf{a}_r is the amplitude, \mathbf{b}_r is the frequency, and \mathbf{c}_r is the horizontal phase constant at each sine wave term. For example, when the profile model is considered as the sum of two sine functions, it could be represented as follows:

$$y_{jp} = a_{1p} \sin(b_{1p} x_{jp} + c_{1p}) + a_{2p} \sin(b_{2p} x_{jp} + c_{2p}) + \varepsilon_{jp} \quad (13)$$

where x_{jp} is the explanatory variable for the j th observation in the p th profile, $\hat{\beta}_p$ is the unknown parameter vector for profile p ($\hat{\beta}_p' = [a_{1p}, a_{2p}, b_{1p}, b_{2p}, c_{2p}, c_{2p}]$), and the error term is independent and identically distributed as a normal random variable with zero mean and constant variance (σ^2).

Then, linear discriminant analysis (LDA) was used with the Hotelling T^2 control chart to monitor the sound frequency signal. The Hotelling T^2 control chart is a multivariate statistical method for quality control, which is an extension of the average control chart by Shewhart [23].

The Hotelling T^2 control chart can be described as follows. The multivariate T^2 control chart was used to monitor the parameter vector ($\hat{\beta}_p$) from the different MSE curve. Then, the T^2 control statistic was calculated as follows:

$$T_p^2 = (\hat{\beta}_p - \bar{\beta})' \mathbf{S}^{-1} (\hat{\beta}_p - \bar{\beta}), \quad p = 1, 2, \dots, g \quad (14)$$

where \mathbf{S} denotes the covariance matrix $\mathbf{S} = \sum_{j=1}^g (\hat{\beta}_j - \bar{\beta})(\hat{\beta}_j - \bar{\beta})' / (g - 1)$ of the profile sample, and g denotes the number of the sound frequency signal profile. Therefore, if a sound frequency signal is classified as abnormal, the MSE parameters of normal and abnormal sound frequencies can be used for classification by LDA as well as the establishment of the control limit.

The classification structure is as follows. First, the control limit for LDA is constructed [24]. The slope w_c and intercept w_{c0} of the control limit can be obtained as follows:

$$g_c(\beta) = w'_c \beta + w_{c0} \begin{cases} > 0, & \text{if } \beta \in \text{Group 1} \\ < 0, & \text{if } \beta \in \text{Group 2} \end{cases} \quad (15)$$

In Equation (15), $g_c(\beta)$ is the linear combination for the upper control limit. The Fisher theory was used to establish the control limit. The norm was defined as the percentage value for the calculated inter- and intra-group variance. The slope w_c of the control limit was obtained by calculating this norm.

$$J_F = \frac{\left|w'_c(m_1 - m_2)\right|^2}{w'_c \Sigma_W w_c} \quad (16)$$

Equation (16) was used to obtain w_c when J was a maximum. m_1 and m_2 denote the means of different groups, and Σ_W denotes the pooled within-class sample covariance matrix:

$$\Sigma_W = \frac{1}{n-2} (n_1 \hat{\Sigma}_1 + n_2 \hat{\Sigma}_2) \quad (17)$$

$\hat{\Sigma}_1$ and $\hat{\Sigma}_2$ denote the maximum-likelihood estimate covariance matrices ($n_1 + n_2 = n$) for type 1 ($\omega_{\text{Group } 1}$) (abnormal frequency) and type 2 ($\omega_{\text{Group } 2}$) (normal frequency), respectively. The maximum slope w_c in Equation (16) can be determined as follows:

$$\frac{w'_c(m_1 - m_2)}{w'_c \Sigma_W w_c} \left\{ 2(m_1 - m_2) + \left(\frac{w'_c(m_1 - m_2)}{w'_c \Sigma_W w_c} \Sigma_W w_c \right) \right\} = 0 \quad (18)$$

$w'_c(m_1 - m_2) / w'_c \Sigma_W w_c$ is a scalar value; thus, it must exist in $w_c \propto \Sigma'_c(m_1 - m_2)$. The above classification steps were applied to convert the MSE parameters of the different sound frequency signals so as to construct the upper control limit in the T^2 control chart.

2.4. Validation

The proposed method was applied to two case studies for validation. In the first case study, the proposed method was applied to a simulation experiment, in which high-, medium-, and low-frequency abnormal data were added to normal data. In the second case study, the proposed method was applied to the analysis of electrocardiography (ECG) signals in a database.

2.4.1. Case Study I: Simulation Experiment

The simulation experiment considered 300 s. of sound frequency signals comprising 20 copies of normal sound frequencies. Two copies of 60-s.-long abnormal sound frequencies were added. Herein, the signals of 100 s. were intercepted and displayed as in Figure 3. Then, EMD was applied to the original signals to obtain the IMFs and residuals of different frequency sections. Figure 3 presents the IMF vectors of the original sound frequency signals after EMD.

The original signals were decomposed into 15 IMFs and one residual; then, the recombined sound frequency signals of IMFs 1–10 were selected for analysis. Then, Equations (9) and (10) were used to convert the signals into MSE values. The third- to fifth-degree polynomial models, the first- to third-degree sums of the sine equations, and the three-stage second-degree polynomial model were evaluated for model fitting. \bar{R}_{adj}^2 was used as an evaluation criterion. \bar{R}_{adj}^2 is the mean of R_{adj}^2 , which is a modified version of R^2 that is adjusted according to the number of predictors in the model. R_{adj}^2 increases when a new predictor improves the model more than expected by chance and decreases when a predictor improves the model less than expected. In contrast, R^2 increases with the number of predictors whether or not they are significant.

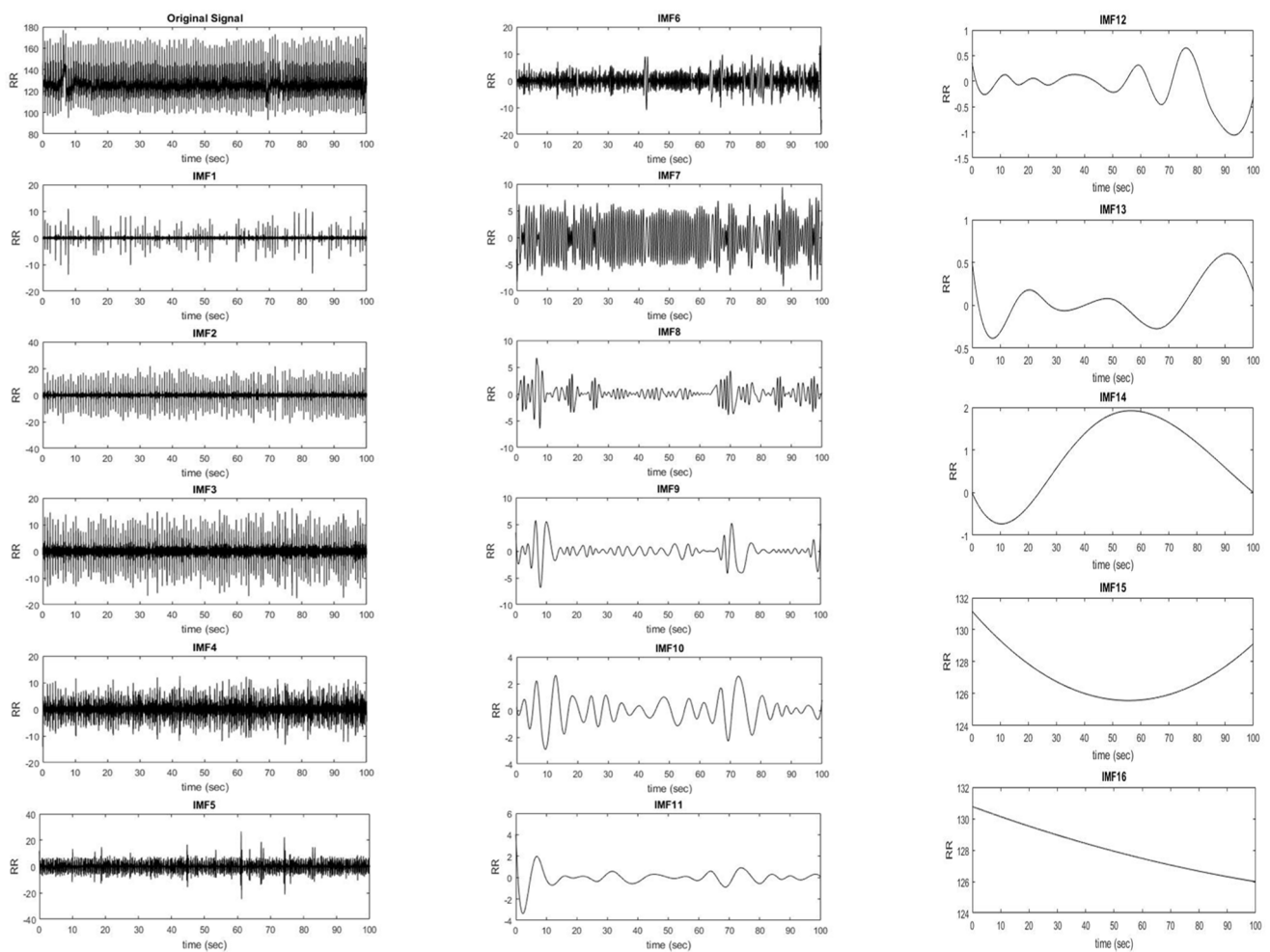


Figure 3. Decomposition of the original sound frequency signals.

2.4.2. Case Study II: Electrocardiography Data

For this case study, 24 lead-I ECG signals were selected as the original data, and two signals contained arrhythmia. The original signals were decomposed to obtain eight IMFs of different frequency bands and one residual, as presented in Figure 4. After combining different IMFs, IMF2, IMF3, and IMF4 were found to have a strong ability to distinguish abnormal signals.

Frequency bands from IMF2 to IMF4 were used to reconstruct the ECG signals for analysis. Then, the reconstructed signals were converted into MSE profiles using Equations (9) and (10). Using the simulated evaluation, the fourth-degree polynomial model was used for model fitting:

$$y_p = \beta_{0p} + \sum_{r=1}^4 \beta_{rp} x^r + \varepsilon_p, \quad p = 1, 2, \dots, q \quad (19)$$

where β_{0p} and β_{rp} denote the estimated parameters of the fourth-degree polynomial model. r is the number of scales, and $\varepsilon_p \sim N(0, \sigma^2)$.

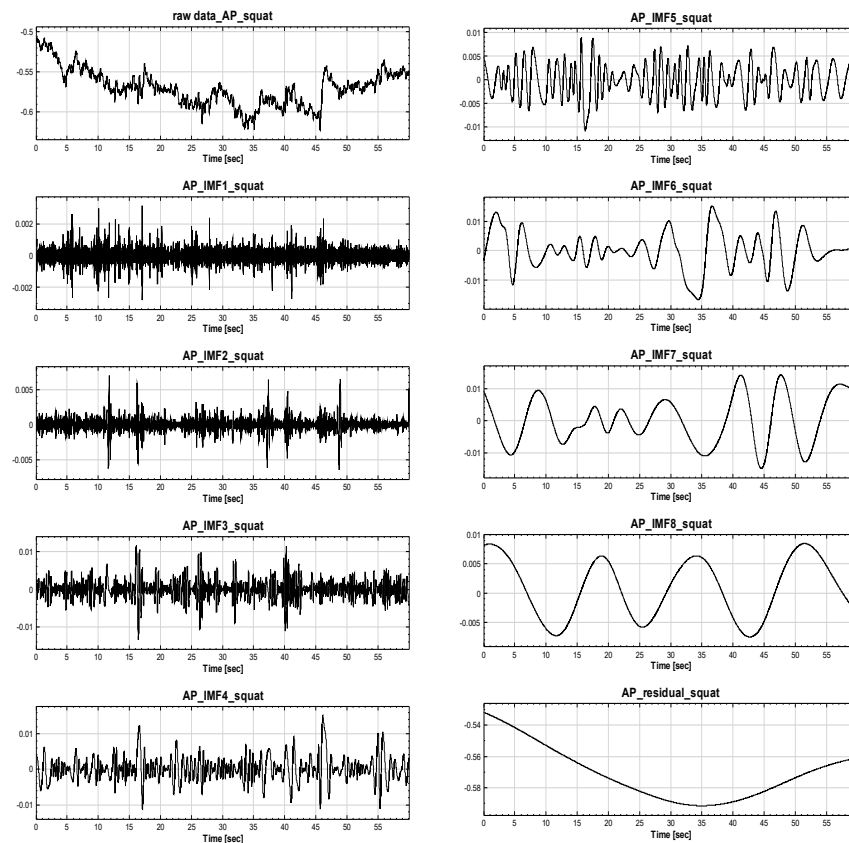


Figure 4. The schematic diagram for the decomposition of the original signals.

3. Results and Discussion

3.1. Case Study I

Table 1 presents the fitting results of the different models to the signals, which were decomposed into 20 groups of mean MSE profiles. The fourth-degree and three-stage second-degree polynomial models had \bar{R}_{adj}^2 values of 0.9603 and 0.9712, respectively. Thus, they demonstrated the best fitting results, which were attributed to the smooth curves of the MSE profiles. The three-stage second-degree polynomial model performed slightly better than the fourth-degree polynomial model due to the smaller number of parameters used in this study. Based on its reduction of the type 1 deviation and convenience of use, the fourth-degree polynomial model was selected for profile monitoring in the simulation experiment.

Table 1. Results of the MSE curve model fitting by polynomial models.

	\bar{R}_{adj}^2
3-order polynomial model	0.9241
4-order polynomial model	0.9603
5-order polynomial model	0.9594
1-sine model	0.8513
2-sine model	0.9214
3-sine model	0.9011
Three-sectioned 2-stage polynomial model	0.9712

To construct a reasonable control line, the original and normal sound frequency signals were mixed with high-, medium-, and low-frequency abnormal sound frequencies, where the signal amplitude was varied at different scales to generate 200 copies of simulated sound frequency signals. Specifically, 10 copies of abnormal sound frequencies in each

frequency domain were chosen for repeated simulation. Four scenarios of sound anomalies were considered: high, medium, low, and mixed frequencies. Table 2 presents the results of repeated random testing. The results indicate that the proposed method detected the anomalies with an accuracy of over 90%. The original signal was detected with an accuracy of less than 50%; thus, it was judged as unidentifiable.

Table 2. LDA Classification-based control limit and accuracy of monitoring abnormal sound frequency.

Different Types of Abnormal Sound Frequency	Transforming Pattern	Accuracy
Abnormal sound for high frequency	Construct the profile to use EMD procedure via the LDA classification of high frequency	96.28%
	Construct the profile to use original signal via the LDA classification of high frequency	Unidentifiable
Abnormal sound for intermediate frequency	Construct the profile to use EMD procedure via the LDA classification of intermediate frequency	94.48%
	Construct the profile to use original signal via the LDA classification of intermediate frequency	Unidentifiable
Abnormal sound for low frequency	Construct the profile to use EMD procedure via the LDA classification of low frequency	95.15%
	Construct the profile to use original signal via the LDA classification of low frequency	Unidentifiable

3.2. Case Study II

Table 3 presents the fitting results of the 24 MSE profiles derived from Equation (19). The minimum, maximum, and average values of R^2_{adj} for all models were 0.97, 0.99, and 0.9846, respectively, which validates the proposed method.

Table 3. The fitting results of MSE curves using the fourth-degree polynomial model.

Sample	1	2	3	4	5	6	7	8	9	10
R^2	0.9902	0.9886	0.9903	0.9910	0.9874	0.9897	0.9911	0.9901	0.9788	0.9888
R^2_{adj}	0.9872	0.9813	0.9869	0.9896	0.9813	0.9815	0.9897	0.9899	0.9704	0.9817
Sample	11	12	13	14	15	16	17	18	19	20
R^2	0.9909	0.9910	0.9913	0.9874	0.9901	0.9895	0.9899	0.9885	0.9913	0.9905
R^2_{adj}	0.9889	0.9887	0.9896	0.9827	0.9891	0.9808	0.9832	0.9803	0.9881	0.9843
Sample	21	22	23	24						
R^2	0.9889	0.990	0.9876	0.9914						
R^2_{adj}	0.9834	0.9811	0.9809	0.9897						

Abnormal and normal MSE profiles for the ECG signals were classified according to the five parameters ($\beta_0, \beta_1, \beta_2, \beta_3, \beta_4$) of the fourth-degree polynomial model and LDA technique. The normal and abnormal profiles were distinguished with a detection accuracy of 100%. The results were utilized to establish the Hotelling T^2 control chart for online anomaly detection. Figure 5 demonstrates that Profiles 6 and 11 exceeded the control line. These two profiles corresponded to abnormal ECG signals in the original data. Thus, the proposed method can be used to detect abnormal ECG signals with excellent sensitivity. In this case, because the ECG signals were non-steady and nonlinear, Fourier analysis could not be applied. EMD was combined with IMF to handle the original lead-I ECG signals, similar to a noise filtering function, and the reconstructed signals were converted into MSE profiles to classify abnormal signals. The parameters of the fourth-order polynomial model were used to accurately monitor abnormal signals.

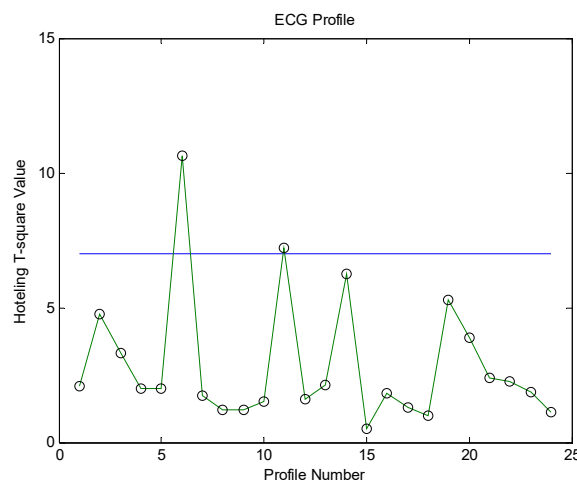


Figure 5. On-line monitoring results of ECG MSE profiles.

To verify the detective performance for the proposed monitoring system, the abnormal signal of lead-I for irregular heartbeat was also tested to obtain the evaluated results. A rational control limit was established to adopt 60 signals of two sources: irregular heartbeat (20 sample signals) and normal ECG signals (40 sample signals) via LDA classification. The database for simulated ECG signals included 160 normal signals and 40 abnormal signals for an irregular heartbeat. Each simulation randomly sampled 80 normal ECG signals and 20 abnormal signals to implement the detective task. Using the simulations of 10 repetitions, the accuracy rate was calculated and the detective performance was evaluated. The results of the repeated random tests are shown in Table 4. According to Table 4, the accuracy of over 65% was achieved in monitoring irregular heartbeats, whether or not the EMD procedure was applied. However, it was also found that the utilized EMD procedure improved significantly. Comparing Table 4 and Figure 5, if the control limit was constructed to use the samples of a lower proportion, it also induced an inferior detection effect. Therefore, the EMD procedure and the control limit to be established are the critical operations and display a significant influence.

Table 4. Adopting the LDA control limit; the accuracy of monitoring irregular heartbeats.

Type of Signals	Profile Transformation	Accuracy Rate
Normal ECG signals	Profile transformation using EMD	97.92%
	Profile transformation using original signal	71.42%
Irregular heartbeat	Profile transformation using EMD	92.20%
	Profile transformation using original signal	65.52%

4. Conclusions

In this study, EMD was combined with IMF to process original signals and analyze the frequency domains for abnormal signals. The following conclusions were obtained:

1. The sound and vibration frequency signals were complex and unstable, but EMD removed unexpected signals and detected abnormal ones. Even when abnormal frequencies were placed at different time points, EMD was more effective than directly converting the original signal into an MSE profile. This demonstrates that monitoring a specific sound frequency indeed improves the identification of abnormal sound frequencies. The proposed method could also be applied to ECG signals.
2. Good model fitting was obtained by converting the MSE profile into a fourth-order polynomial model. Although a complex model has a better fit than the third-order polynomial model, the latter is still advantageous owing to its fewer parameters and highly accessible LDA classification structure.

Although the selection of IMF vectors for signal combination and reconstruction is a critical procedure for monitoring sound frequency and ECG signals, it is still impossible to obtain high sensitivity if IMF vectors with features that can be clearly identified or excessive original signals are removed. The IMF selection procedure still needs to be improved. In future research, the proposed method may be combined with deep learning to obtain better combinations of sound frequency signals (or ECG data). Because signals reconstructed with EMD are easier to identify, multivariate control charts would be helpful for online monitoring if combined with a better IMF selection and reconstruction theory. However, different control graphs have different degrees of sensitivity. Therefore, another future research topic is combining classification processes and selecting a control graph with a lower probability of deviation.

Author Contributions: Conceptualization, C.-H.J. and C.-C.W.; methodology, C.-H.J. and C.-C.W.; validation, C.-H.J. and C.-C.W.; formal analysis, C.-H.J. and C.-C.W.; data curation, C.-H.J.; writing—Original draft preparation, C.-H.J. writing—review and editing, C.-C.W. and C.-H.J. All authors have read and agreed to the published version of the manuscript.

Funding: This research received no external funding.

Institutional Review Board Statement: Not applicable.

Informed Consent Statement: Not applicable.

Data Availability Statement: Not applicable.

Conflicts of Interest: The authors declare no conflict of interest.

References

1. Dai, X.W.; Gao, Z.W. From model, signal to knowledge: A data-driven perspective of fault detection and diagnosis. *IEEE Trans. Ind. Inform.* **2013**, *9*, 2226–2238. [[CrossRef](#)]
2. Yan, K.; Ji, Z.; Shen, W. Online fault detection methods for chillers combining extended kalman filter and recursive one-class SVM. *Neurocomputing* **2017**, *228*, 205–212. [[CrossRef](#)]
3. Sun, K.Z.; Li, G.N.; Chen, H.X.; Liu, J.Y.; Li, J.; Hu, W.J. A novel efficient SVM-based fault diagnosis method for multi-split air conditioning system's refrigerant charge fault amount. *Appl. Therm. Eng.* **2016**, *108*, 989–998. [[CrossRef](#)]
4. Rogers, A.P.; Guo, F.; Rasmussen, B.P. A review of fault detection and diagnosis methods for residential air conditioning systems. *Build. Environ.* **2019**, *161*, 106236. [[CrossRef](#)]
5. Gangsar, P.; Tiwari, R. Signal based condition monitoring techniques for fault detection and diagnosis of induction motors: A state-of-the-art review. *Mech. Syst. Signal Process.* **2020**, *144*, 106908. [[CrossRef](#)]
6. Neupane, D.; Seok, J. Bearing fault detection and diagnosis using Case Western Reserve University dataset with deep learning approaches: A review. *IEEE Access* **2020**, *8*, 93155–93178. [[CrossRef](#)]
7. Fan SK, S.; Hsu, C.Y.; Jen, C.H.; Chen, K.L.; Juan, L.T. Defective wafer detection using a denoising autoencoder for semiconductor manufacturing processes. *Adv. Eng. Inform.* **2020**, *46*, 101166. [[CrossRef](#)]
8. Fan SK, S.; Tsai, D.M.; He, F.; Huang, J.Y.; Jen, C.H. Key parameter identification and defective wafer detection of semiconductor manufacturing processes using image processing techniques. *IEEE Trans. Semicond. Manuf.* **2019**, *32*, 544–552. [[CrossRef](#)]
9. Shao, X.; Barker, J. Stream weight estimation for multistream audio–visual speech recognition in a multispeaker environment. *Speech Commun.* **2008**, *50*, 337–353. [[CrossRef](#)]
10. Xie, C.; Cao, X.; He, L. Algorithm of abnormal audio recognition based on improved MFCC. *Procedia Eng.* **2012**, *29*, 731–737. [[CrossRef](#)]
11. Nalini, S.A.; Yusuf, D.J.; Alan Mackinnon, B. Application of acoustic directional data for audio event recognition via HMM/CRF in perimeter surveillance systems. *Robot. Auton. Syst.* **2015**, *72*, 15–28.
12. Nalini, N.J. Music emotion recognition: The combined evidence of mfcc and residual phase. *Egypt. Inform. J.* **2016**, *17*, 1–10. [[CrossRef](#)]
13. Lee, Y.C.; Shariatfar, M.; Rashidi, A.; Lee, H.W. Evidence-driven sound detection for prenotification and identification of construction safety hazards and accidents. *Autom. Constr.* **2020**, *113*, 103127. [[CrossRef](#)]
14. Liu, Z.; Li, S. A sound monitoring system for prevention of underground pipeline damage caused by construction. *Autom. Constr.* **2020**, *113*, 103125. [[CrossRef](#)]
15. Wei, J.; Wang, Z.; Xing, X. A Wireless High-Sensitivity Fetal Heart Sound Monitoring System. *Sensors* **2021**, *21*, 193. [[CrossRef](#)]
16. Huang, N.E.; Shen, Z.; Long, S.R.; Wu, M.C.; Shih, H.H.; Zheng, Q.; Yen, N.C.; Tung, C.C.; Liu, H.H. The empirical mode decomposition and the Hilbert spectrum for nonlinear and non-stationary time series analysis. *Proc. R. Soc. Lond.* **1998**, *454*, 903–995. [[CrossRef](#)]

17. Pachori, R.B.; Avinash, P.; Shashank, K.; Sharma, R.; Acharya, U.R. Application of empirical mode decomposition for analysis of normal and diabetic RR-interval signals. *Expert Syst. Appl.* **2015**, *42*, 4567–4581. [[CrossRef](#)]
18. Safi, K.; Mohammed, S.; Albertsen, I.M.; Delechelle, E.; Amirat, Y.; Khalil, M.; Gracies, J.M.; Hutin, E. Automatic analysis of human posture equilibrium using empirical mode decomposition. *Signal Image Video Process.* **2017**, *11*, 1081–1088. [[CrossRef](#)]
19. Alickovic, E.; Kevric, J.; Subasi, A. Performance evaluation of empirical mode decomposition, discrete wavelet transform, and wavelet packed decomposition for automated epileptic seizure detection and prediction. *Biomed. Signal Process. Control* **2018**, *39*, 94–102. [[CrossRef](#)]
20. Wang, C.C.; Jiang, B.C.; Huang, P.M. The relationship between postural stability and lower-limb muscle activity using an entropy-based similarity index. *Entropy* **2018**, *20*, 320. [[CrossRef](#)]
21. Wang, C.C.; Jiang, B.C.; Lin, W.C. Evaluation of effects of balance training from using wobble board-based exergaming system by MSE and MMSE techniques. *J. Ambient. Intell. Humaniz. Comput.* **2018**, *9*, 1745–1754. [[CrossRef](#)]
22. Costa, M.; Goldberger, A.L.; Peng, C.K. Multiscale entropy analysis of biological signals. *Phys. Rev. E* **2005**, *71*, 021906-1–021906-18. [[CrossRef](#)] [[PubMed](#)]
23. Riaz, M.; Saeed, U.; Mahmood, T.; Abbas, N.; Abbasi, S.A. An improved control chart for monitoring linear profiles and its application in thermal conductivity. *IEEE Access* **2020**, *8*, 120679–120693. [[CrossRef](#)]
24. Fu, R.; Tian, Y.; Bao, T.; Meng, Z.; Shi, P. Improvement motor imagery EEG classification based on regularized linear discriminant analysis. *J. Med. Syst.* **2019**, *43*, 169. [[CrossRef](#)] [[PubMed](#)]